AIP | Review of Scientific Instruments

An in-vacuo optical levitation trap for high-intensity laser interaction experiments with isolated microtargets

C. J. Price, T. D. Donnelly, S. Giltrap, N. H. Stuart, S. Parker, S. Patankar, H. F. Lowe, D. Drew, E. T. Gumbrell, and R. A. Smith

Citation: Review of Scientific Instruments **86**, 033502 (2015); doi: 10.1063/1.4908285
View online: http://dx.doi.org/10.1063/1.4908285
View Table of Contents: http://scitation.aip.org/content/aip/journal/rsi/86/3?ver=pdfcov
Published by the AIP Publishing

An *in-vacuo* optical levitation trap for high-intensity laser interaction experiments with isolated microtargets

C. J. Price,[1,a)] T. D. Donnelly,[2] S. Giltrap,[1] N. H. Stuart,[1] S. Parker,[1] S. Patankar,[1] H. F. Lowe,[1] D. Drew,[3] E. T. Gumbrell,[3] and R. A. Smith[1]
[1]*Blackett Laboratory, Imperial College, London SW7 2AZ, United Kingdom*
[2]*Department of Physics, Harvey Mudd College, Claremont, California 91711, USA*
[3]*Radiation Physics, AWE, Aldermaston, Reading, Berkshire RG7 4PR, United Kingdom*

(Received 24 November 2014; accepted 4 February 2015; published online 6 March 2015)

We report on the design, construction, and characterisation of a new class of *in-vacuo* optical levitation trap optimised for use in high-intensity, high-energy laser interaction experiments. The system uses a focused, vertically propagating continuous wave laser beam to capture and manipulate micro-targets by photon momentum transfer at much longer working distances than commonly used by optical tweezer systems. A high speed (10 kHz) optical imaging and signal acquisition system was implemented for tracking the levitated droplets position and dynamic behaviour under atmospheric and vacuum conditions, with ±5 μm spatial resolution. Optical trapping of 10 ± 4 μm oil droplets in vacuum was demonstrated, over timescales of >1 h at extended distances of ~40 mm from the final focusing optic. The stability of the levitated droplet was such that it would stay in alignment with a ~7 μm irradiating beam focal spot for up to 5 min without the need for re-adjustment. The performance of the trap was assessed in a series of high-intensity (10^{17} W cm^{-2}) laser experiments that measured the X-ray source size and inferred free-electron temperature of a single isolated droplet target, along with a measurement of the emitted radio-frequency pulse. These initial tests demonstrated the use of optically levitated microdroplets as a robust target platform for further high-intensity laser interaction and point source studies. [http://dx.doi.org/10.1063/1.4908285]

I. INTRODUCTION

The interaction of an intense laser pulse with micron-sized, mass-limited targets has the potential to create low debris, low electromagnetic pulse (EMP), high-brightness X-ray or fast particle sources.[1–3] A mass-limited target is defined as an object not in direct contact with any surrounding matter (e.g., a mounting pin) and where energy transport mechanisms, such as thermal and hot electron currents are spatially confined. Such sources have a broad range of potential applications, including generating and probing high energy density plasmas and materials under extreme conditions. For particles of order, the laser wavelength, Mie-like resonances can also result in significant "geometric" enhancement of the laser electric field over the surface of the target, potentially increasing coupling efficiency and enhancing hot-electron temperatures.[4,5]

In an unsupported target, strong laser-driven electric fields can be established over the target surface and these, in turn, couple to hot electron generation and ion acceleration processes.[6–11] Eliminating a physical support structure also prevents the generation of unwanted X-ray or particle sources from hot-electron transport into surrounding matter, e.g., a support pin. The lack of a physical return current path for electrons ejected from the target and subsequently captured by the vacuum chamber wall may also greatly reduce potentially damaging EMP generation. In high energy, petawatt-class experiments, EMP emission from the large electric currents created with "standard" pin-mounted targets can be a limiting process for the use of sensitive electronic systems, e.g., CCD cameras and gated imaging devices. Reducing EMP is therefore of potential benefit to experiments at major laser facilities such as the National Ignition Facility.[12,13] Due to these compelling advantages, levitated targets have a number of exciting potential applications. For example, as sources for high resolution X-ray and particle imaging due to their micron-scale size and high energy X-ray emission, low debris, expected high (sub-ps) time-resolution, and low EMP.

Alternative mass-limited target injection techniques have been previously demonstrated using sprays from pulsed nozzles[14] and jets of fast moving liquid droplets.[15] These methods are well matched to small-scale, high repetition rate lasers, but not for lower repetition rate, very high energy systems. Here, the setup and operating "cost" of individual shots can be significant and therefore demands a highly reliable target platform that ensures target alignment to the high-power laser focus. Direct spatial control of the target is also crucial, as is the ability to fully characterise or exploit the laser-target interaction with a diagnostic suite occupying multiple viewing angles. These requirements generate a set of constraints that motivated the development of the new *in-vacuo* optical levitation trap we present here. It will enable well-defined investigations into laser-microtarget interactions at the highest intensities available from petawatt-class facilities. An additional motivating factor is the potential

a)Electronic mail: c.price10@imperial.ac.uk

to achieve local boosts to the laser driven electric field of order 10-1000 for arrays of space fixed microtargets,[16] potentially extending petawatt class experiments to the exawatt regime by harnessing geometric boosts to the local electric field.

There has been research into the use of electrostatic traps to levitate particles for the kinds of interaction experiments we describe,[17,18] but these studies addressed ion emission and acceleration, and employed a fundamentally different trapping mechanism and geometry to the one we present here. As the electrostatically levitated target is held within a Paul trap, the accessible viewing angles are greatly restricted by the surrounding electrodes and thus limit diagnostic access or the ability to use a trapped particle as a source for imaging applications. Particles must also be charged to be confined in electrostatic systems and a sophisticated optical feedback system is required for good spatial control. The particle must also be a solid rather than a liquid as electrostatic forces can otherwise cause a charged droplet to break up.[19]

In this paper, we report on the development of a new class of optical levitation trap optimised to confine few micron objects in vacuum over extended timescales and at large (~40 mm) working distances with a position accuracy of a few microns. This will, for the first time, allow optically levitated, electrically neutral, isolated micro-targets to be irradiated at very high intensity using large, low repetition rate national facility scale laser systems.

A. Optical levitation

When light is reflected or refracted by small particles, photons undergo a change in momentum, and this, in turn, is coupled to the particle. These changes in momentum produce forces that form the basis of optical trapping. This phenomenon is well understood with pioneering the work by Nichols, Hull,[20] and Lebedev[21] who successfully measured the effect of radiation pressure on macroscopic objects and absorbing gases. This was extended in 1970 by Ashkin[22] with his seminal paper on the acceleration and manipulation of micron-sized particles. Ashkin's work demonstrated the trapping of a range of microscopic objects including solid glass spheres, hollow dielectric spheres, and liquid micro-droplets.[23,24] It was also shown that these particles could be trapped under high vacuum conditions (down to ~10^{-6} Torr) with measurements carried out to investigate the unique dynamics exhibited by particles at these low pressures.[25] Optical trapping at small (few mm) working distances in a fluid medium is now a ubiquitous and widely used technique. However, *in-vacuo* levitation has received little attention and has only recently been exploited, e.g., over very short working distances to enable elegant experiments on rotating birefringent particles.[26]

II. OPTICAL TRAP DESIGN

A trapping system optimised for high-intensity laser interaction experiments is subject to several key design constraints. Plasma self-emission and scattered high-intensity laser light can damage optics in close proximity to the interaction region. Conventional trapping systems based on high numerical aperture, multi-element microscope objectives cannot, therefore, be used. Such optics have glued components and are highly vulnerable to laser induced damage if high-intensity light is coupled into the system. Our solution uses a large working distance, high-damage threshold singlet lens with the additional benefit of a large field of view for diagnostic access and applications. The trap must also operate for extended (multi-hour) periods under vacuum to accommodate target chamber pump-down and alignment of a high-energy laser and multiple plasma diagnostic systems. Thus, few micron position stability of the trapped particle is a specific requirement for the system, as is the ability to trap particles that can survive in low pressure environments.

The trapping system implemented is based on 2 in. diameter singlet optical elements with a long focal length aspheric (f = 40 mm, NA ~ 0.52) as the final focussing lens, producing a measured focal spot of 3 μm (FWHM). This system provided viewing access of ~92% of the full 4π sr solid angle around the trapped target. A 5 W, 532 nm continuous wave (CW) laser (Coherent Verdi) was used as the trapping source and was injected into the trap via a single-mode optical fibre to provide a high-quality Gaussian spatial profile with ~1% RMS power stability. A waveplate, Pockels cell, and polariser allowed static and dynamic power control into the fibre (Figure 1(a)). The trap assembly was mounted on a 60 mm cage system to allow for pre-alignment and installation in a range of test environments (Figure 1(b)).

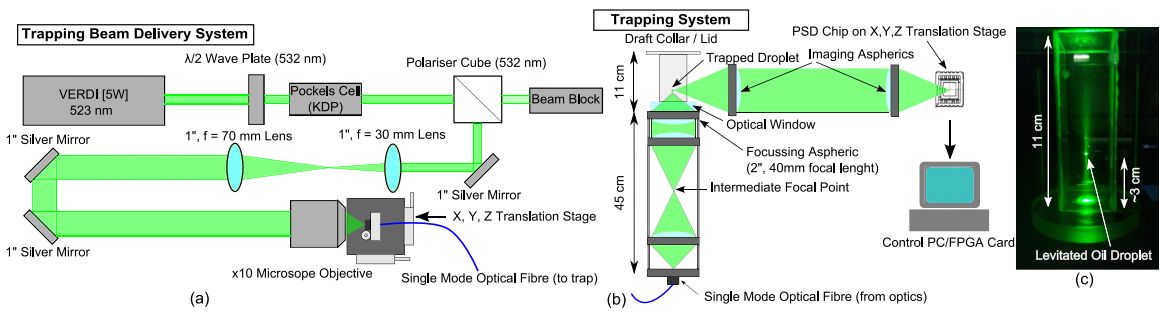

FIG. 1. (a) The trapping beam delivery system was based on a 5 W, 523 nm CW laser. The beam passed through a waveplate, Pockels cell, and polariser allowing static and real time power control. This was coupled into a single mode optical fibre via a 10× objective, with light delivered to the trap remotely by the fibre. (b) The system used to trap both salt and oil microdroplets. The design incorporates an intermediate focus for use with a plasma shutter for damage mitigation. (c) A trapped droplet inside a rectangular draft collar, sitting on the final optical window of the trapping system. The diffraction pattern produced from the trapped droplet can be seen on the underside of the collar lid.

A. Trapping in air

Initial levitation experiments were performed at atmospheric pressure, using saturated salt water test droplets. Using the system detailed in Figure 1, we were able to trap droplets of order 7-10 μm for many hours at a time with ~100-120 mW of optical power delivered to the trapping region. These droplets were generated by a commercial mesh nebuliser (Prowave M2313500), operating with a frequency of ~143 kHz. An intermediate focus was included in the initial optical design for potential use with a fast plasma shutter, or "optical fuse," to block high-intensity laser light or self-emission from laser-heated plasmas[27,28] that might otherwise back propagate through the trapping system and damage elements such as the output face of the optical fibre. A section of collimated beam path within the trapping system also allowed for narrow-band optical filtering to minimise propagation of unwanted radiation back to the fibre. An optically flat anti-reflection (AR) coated glass plate in front of the aspheric prevented mechanical damage by plasma or target debris and accumulation of material during trap loading. A cylindrical collar, 11 cm in length and 2 cm in diameter, was placed around the trapping region to act as a draft shield, without which trapping was found to be challenging due to local air currents. The system was loaded with an air suspension (mist) of droplets falling under gravity through the trap focus. The size of the droplets was sufficiently small that they remained in suspension for several minutes, allowing easy handling. The collar protected droplets from local air currents once trapped and also guided the mist into a narrow, concentrated stream that aided loading. The use of a long collar allowed the top to be closed with a glass plate before droplets reached the trapping region, which proved critical for the loading and sustained trapping in air. If both ends of the collar were open, the "stack effect"[29–31] produced upward thermal currents, driven by the trapping laser, that rapidly destabilised a trapped particle.

B. Particle tracking system

To study the dynamics of trapped droplets and to provide quantitative measurements of position stability, a high speed, high resolution optical imaging system was implemented. This was based around a Hamamatsu S5990-01 tetralateral position sensitive detector (PSD) that measured the relative position of a droplet using scattered trap light relayed onto the PSD using a 1:1 imaging system. An image of the trapped droplet was projected onto the PSD using a pair of 2 in. aspheric lenses of focal length 100 mm (Figure 1(b)). Analogue current signals from the four corners of the PSD were amplified and then interfaced with a differential line driver (THAT1646) to minimise electrical noise pickup. The differential signals were fed to a remote receiver (OPA1632) and multi-gain pre-amp before being processed using a LabView controlled field-programmable gate array (FPGA) card [NI PXI-4110]. The PSD was mounted on a small daughter board to allow for easy replacement if damaged by high-intensity laser light. The x- and y-positions of the droplet were determined at a sampling rate of 10 kHz and the standard deviation of the position measurement over one second intervals used to give a real-time measure of the noise on the position signals, therefore acting to limit the position resolution. The best position resolution achieved (signal to noise), in air, was ±2 μm in x and y. A feedback control system was established whereby the calculated position of the droplet was used to alter the polarisation of the potassium dihydrogen phosphate (KDP) Pockels cell, and thus the power of the trapping beam, with a bridged duel ±200 V amplifier [LME49830] driven by the NI card analogue output via a proportional-integral-derivative (PID) algorithm.

C. Choice of test droplet composition

Saturated salt water droplets were found to become unstable once the ambient pressure was reduced below 500–300 millibars and so *in vacuo* operation was carried out using low vapour pressure, high boiling point oils. A number of oils of varying composition, viscosity, and refractive index were assessed and droplets produced using a Sonear Ultrasonics high frequency (~130 kHz) atomising nozzle generating a size distribution centred at ~10 μm (for water). Operational limitations of the atomiser prevented the use of oil with viscosities greater than 50 cSt. The oil used for low pressure tests was Kurt J Lesker 704 Silicon Pump Fluid ($C_{28}H_{32}Si_3O_2$) with a viscosity of 37 cSt at 25 °C. Stable levitation of ~10 μm droplets of this oil was achieved using ~370–400 mW of optical power in the trapping region, and it was found that once trapped, the power could be reduced to around 40 mW. Trapping life times in air were in excess of 5 h.

The size of trapped oil droplets was determined using the diffraction pattern formed directly above the trap (Figure 2). The size of the droplet could be found using the far-field (Fraunhofer) diffraction from a circular aperture. This gives rise to an Airy diffraction pattern, where the angle subtended by the centre of the first central (maxima) zone to the first minima is given by $\sin\theta = 1.22\lambda/D$, where λ is the laser wavelength and D the aperture (or droplet) diameter. This method was found to work well for droplets larger than ~14 μm but below this a minima was seen in the central zone of the diffraction pattern. For smaller droplets approaching the wavelength of the trapping laser, the diffraction patterns become more complex as optical scattering takes place in the Mie regime and are strongly angularly dependant. A second method of measuring the trapped droplet size was developed using a 100× microscope objective to view the focussed 1:1 image of the droplet produced by the 90° side imaging system. It was observed that at this magnification, the upper and lower scatter points on a single particle could be resolved, as first observed by Ashkin.[32] The distance between these scatter points provided a good approximation of the droplet size, as given in Figure 2, with relation to the associated diffraction patterns.

As the power of the trapping laser remained constant, it was observed that a range of droplets of different sizes were trapped during loading. By keeping the PSD camera at a fixed position, the relative vertical position of each droplet could be measured. It was found that larger droplets would trap in a lower position (closer to the trapping laser focus) than smaller droplets.

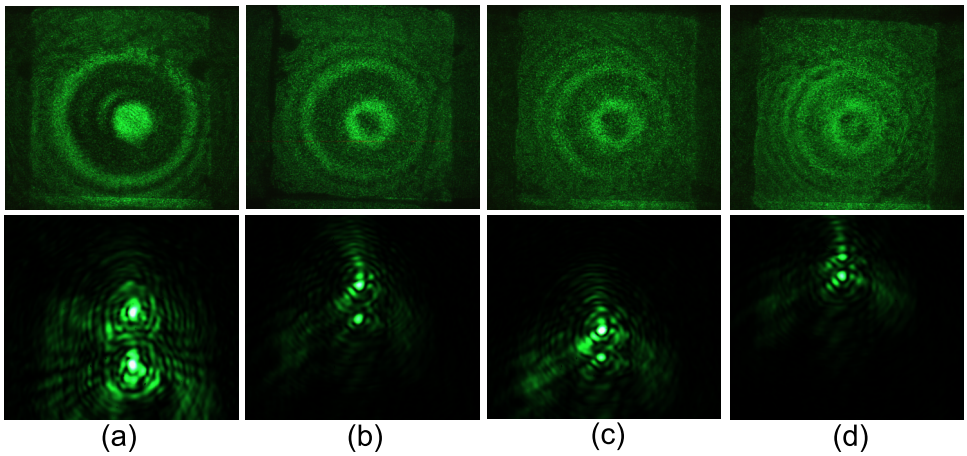

FIG. 2. Optical images of trapped oil microdroplets. For each image pair, the upper image is the vertical far field diffraction pattern produced by the droplet at a distance of 1 m from the trap, and the lower is the 100× magnified 90° image of the droplet. Side imaging reveals two bright spots from the scatter at the top and bottom of the droplet, allowing its approximate size to be determined. Image (a) was measured to be ~14 μm, (b) ~11 μm, (c) ~9 μm, and (d) ~6 μm. The images do not represent the absolute position of each droplet with respect to each other. The aberrations on the side images are due to the scattered light passing through the draft collar.

D. Trapping under vacuum

A more compact version of the trap (Figure 3) was constructed to allow installation in a test vacuum chamber. To reduce the length of the final optical assembly, an f = 70 mm plano-convex lens was used to collimate the beam directly from the output of the fibre before focusing by the aspheric. A 1 μm optical notch filter was placed at the fibre output to reduce back scatter or self-emission from the laser irradiated droplet. Tests with salt water and oil droplets demonstrated that the same conditions of optical power and focal spot size were required to trap using this simplified design, and the stability and lifetime of trapped droplets were comparable. The trap was used with a draft collar mounted on a translation stage to allow removal under vacuum. Loading was conducted at atmosphere and the pressure then reduced. The trap was found to be sensitive to both air currents and vibration while evacuating the chamber and so the pumping rate to pressures down to a few millibars was throttled with a mechanical valve and care taken to isolate vibration from mechanical rotary pumps. To reduce the risk of ambient air molecules destabilising the droplet, the chamber was pumped slowly to this pressure over ~15 min. At this point, the collar could be lifted with no risk of the droplet falling out of the trap, exposing the tapped particle, and the chamber pressure reduced further to $\sim 6 \times 10^{-1}$ millibars where trapping lifetimes of up to 1 h were achievable. As with operation in air, the power of the trapping laser could then be reduced to ~40 mW with the droplet remaining trapped robustly under vacuum.

E. In-trap droplet dynamics

Figure 4 gives the horizontal and vertical positions of a trapped droplet as the chamber was pumped down. Plots (a) and (b) show the vertical displacement of the

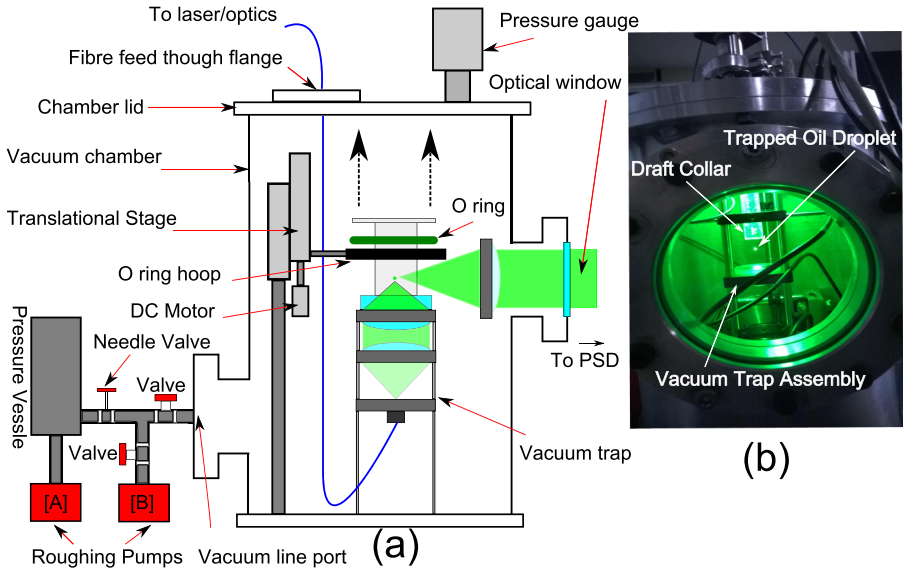

FIG. 3. (a) Vacuum test chamber used for vacuum trapping of oil microdroplets. (b) A view of the loaded vacuum trap (under vacuum) without the imaging optics in place. It can be seen that the draft collar has been removed, and the droplet (small, bright spot at the centre of the image) is unobscured.

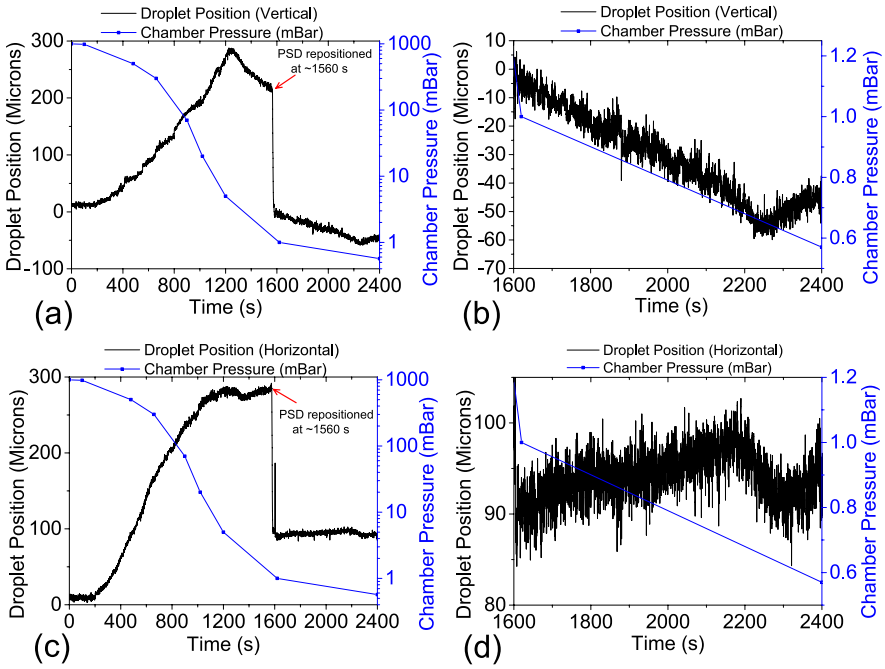

FIG. 4. Plots showing the vertical (a), (b) and horizontal (c), (d) position measurements of a trapped droplet during chamber pump down. The mechanical behaviour of the chamber initially dominates the measured position of the droplet. At t = 1300 s, when the pressure reached ~5 millibars, this effect becomes minimal, and the detailed droplet trap dynamics becomes apparent. Below this pressure, the effect of radiometric forces and the thermal conductivity and viscosity of the surrounding medium reduce, and the dominant forces acting on the droplet are due to photophoresis.

droplet as a function of pressure, and it can be seen that as the pressure falls, the droplet's position beings to rise. This motion is attributed to the vacuum chamber [130 cm diameter, 40 cm height] flexing upwards by ~300 μm as the internal pressure was reduced. When the chamber pressure was at approximately 5 millibars, which correlated with the mean free path of ambient gas becoming comparable to the droplet diameter, the effect of radiometric (thermal) forces of the surround gas on the droplet starts to diminish and the effectiveness of the thermal conductivity of the surrounding atmosphere also drops, potentially resulting in droplet heating. At this pressure, it is thought that the process of negative photophoresis[33] caused the droplet to descend slightly into the levitating beam. Figure 4(b) shows the continued drop in the vertical direction which eventually stopped at ~0.6 millibars and then began to rise again. This rise is attributed to the onset of gradual photochemical damage of the oil, increasing its optical absorption, resulting in positive photophoresis, causing the droplet to rise in the levitating beam.[34] It is thought that it is this effect that, after ~1 h trapping below 5 millibars, finally destabilises the droplet and causes it to fall out of the trap. Figures 4(c) and 4(d) show the droplet's horizontal position as the chamber was pumped down. There was significant horizontal motion (comparable to the vertical motion) of the droplet which we attribute primarily to flexing of the vacuum chamber causing the trapping assembly to tilt slightly. It is interesting to note, however, that the extent of this motion levels-out at the same time and pressure as the point of inflection of the vertical position; this confirms the notion that after this point, all motion can be attributed to the droplet dynamics and not the mechanical behaviour of the vacuum system. During the final 800 s of the measurement (1600–2400 s), with a pressure range from 1.2 to 0.6 millibars, the droplet moves ~50 μm in the vertical direction and only ~10 μm in the horizontal. The measured signal to noise for both the vertical and horizontal position measurements was ±5 μm. The position of the PSD camera was re-set after ~1560 s so that the image of the droplet was approximately at the centre of the chip, giving the best possible measurement (signal to noise).

III. INTENSE LASER INTERACTION EXPERIMENTAL SETUP

A schematic of the configuration for the proof of principle experiments is shown in Figure 5. Optically levitated droplets were irradiated with ~450 fs pulses from a high-contrast hybrid optical parametric chirped-pulse amplification (OPCPA)/Nd:Glass ~1TW (0.3 J) laser system operating at 1054 nm.[35] A 2 in., 20 cm focal length gradient-index (GRIN) lens focused the interaction beam onto target producing a spot size of ~7 μm (FWHM), a Rayleigh range of ~135 μm, and a peak intensity of ~10^{17} W cm^{-2}. To pre-align the laser and plasma diagnostics, a 50 μm wire mounted on a translation stage, horizontally and perpendicular to the irradiating laser beam, was first placed at the target chamber centre. A low power alignment beam collinear with the main heating beam was used for target pre-alignment by obscuration of low intensity light by the wire, as observed by Sumix camera [C].

Steel knife edges were used for penumbral X-ray source size measurements and were placed approximately ~7 cm away from the droplet position. X-ray image plate (Fuji BAS MS2325) was placed ~42 cm from the knife edges giving an M = 6 (magnification) imaging system. A shadow of the edge of the obscuring structures was cast onto the image plate, so that orthogonal edge positions could be accurately imaged.

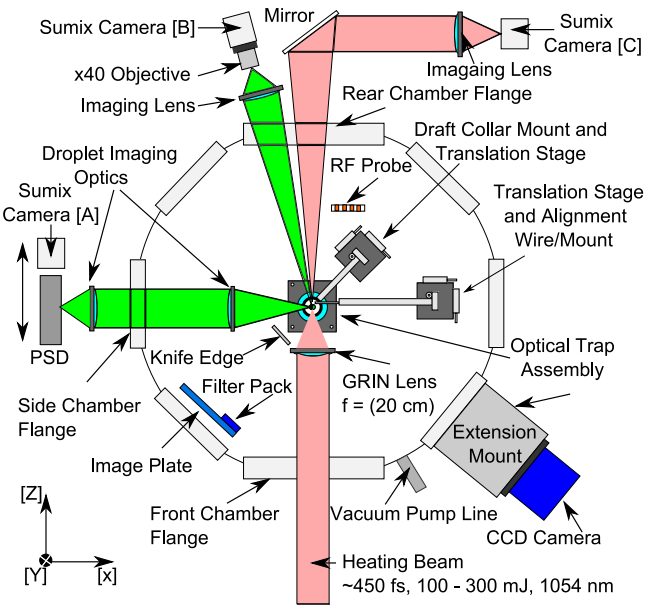

FIG. 5. A schematic of the target chamber, alignment, and diagnostic-layout for the high-intensity laser droplet interaction experiments. Knife-edge diagnostics were used to measure X-ray source size, an Andor CCD camera used as a single hit low-resolution spectrometer for X-ray photons, and a pick-up probe deployed to measure the RF emission. Viewing angles were established to monitor the trapped droplet position (Sumix camera [A] and [B]) and also for accurate alignment with the main heating beam under vacuum (Sumix camera [C]).

A back-thinned X-ray sensitive CCD camera (Andor DO 440) configured as a single-hit energy resolving spectrometer was placed at a distance of ~200 cm to the target chamber centre and located between the 90° alignment wire translation stage and the heating beam. A 25 μm beryllium foil filter shielded the diagnostic from scattered laser light and soft xuv emission <1 keV. A razor blade positioned over part of the CCD chip provided discrimination between background noise and direct X-ray signal from an irradiated target.

To provide a preliminary quantitative analysis of EMP levels,[36,37] a probe consisting of a 6 turn coil of multi-core copper wire covered by a layer of plastic insulation was placed inside the chamber to measure RF pick-up and read out with a 50 Ω terminated, 300 MHz digital oscilloscope.

A. Droplet alignment

The trapping assembly was initially positioned ~1 cm in front of the alignment wire before it was loaded and the chamber sealed and pumped down. When at vacuum, the alignment wire had to be re-aligned to the laser focus due to the chamber flexing during pump down. Two orthogonal viewpoints were established so that scattered IR light from the tip of the wire, and thus the position heating beam focus could be aligned remotely in 3D. This was achieved by marking this position on a camera at 90° to the heating beam line (Sumix camera [A]) and on an imaging system that operated slightly off axis to the heating beam with a 40x microscope objective (Sumix camera [B]). The alignment wire was moved out of the focal region and the trapping assembly then translated, using a 3-axis stage, until the green scattered light from the droplet overlapped the marked target positions on both orthogonal cameras. It was found that when loaded, the system could be translated at ~20 μm s^{-1} without losing the droplet. When relatively close to the focus of the oscillator beam, there was sufficient IR scatter from the droplet from the low power (<1 mW) alignment beam to allow it to be "walked" into the centre of the focal spot. Once positioned in the 7 μm focus of the IR oscillator beam, it was found that the droplet would stay within a focal spot diameter for up to 5 min without the need to readjust its position. It is thought that the main causes of long-timescale misalignment were from power fluctuations in the trapping beam.

IV. INTENSE LASER INTERACTION RESULTS

A. X-ray source size and spectrum

To extract X-ray source sizes from the knife edge data, the image plate was post-processed by a Fuji BAS 1800II reader with a spatial resolution of 20 ± 2 μm, at a magnification of M = 6, for X-ray images projected onto the plate. Figure 6 shows experimental knife edge images produced by irradiating a droplet (a) and a 9 μm diameter carbon wire (d). The source size was determined by measuring the FWHM of a Gaussian curve fitted to the line spread function (LSF) of each edge.

Transmission measurements were taken using differential X-ray filters placed in front of the image plate, consisting of two aluminium foils of 0.8 μm (>300 eV photons) and 1.6 μm (>400 eV photons) across both knife edges, to assess the X-ray source size at different photon energies. Each filter pair, horizontal and vertical, was mounted on a metal ring (visible in Figure 6) and aligned so that they would cover the shadow cast by each of the knife edges. This filtering also blocked soft (<100 eV), thermal X-ray emission with the potential to reduce the resolution of the image plate measurement. Image plate data indicated that the 1.6 μm aluminium filter was sufficient to block all of the emitted X-ray flux from the droplet and so no edge response could be measured through this. Source size comparisons were made between a levitated droplet and a 9 μm carbon wire (irradiated with ~300 mJ laser pulses) to assess the targets' physical and geometrical extent on the measured source size, with the targets having similar atomic composition. The results are shown in Table I.

The droplet gave a source size measurement that was comparable to the ultimate spatial resolution of the imaging system, indicating an X-ray source comparable to its pre-irradiation physical size in both horizontal and vertical orientations. The carbon wire gave a similar result for its vertical source size, however, the horizontal source size was resolvable indicating a larger extended X-ray source. This was thought to be a result of electrons streaming along the length of the wire during the interaction process.[38–40]

An estimate of the time-integrated plasma free electron temperature for the droplet was made by analysing single-hit data from the Andor CCD filtered with 25 μm of beryllium. Fits to energy-binned photon flux (on a log-lin scale) indicated two linear regions corresponding to an upper and lower electron temperature range from 0.4 to 2.3 keV. It is assumed that the droplet expansion was rapid enough that the thermalisation of the plasma occurred over a relatively long period of time, and hence the temperature range is

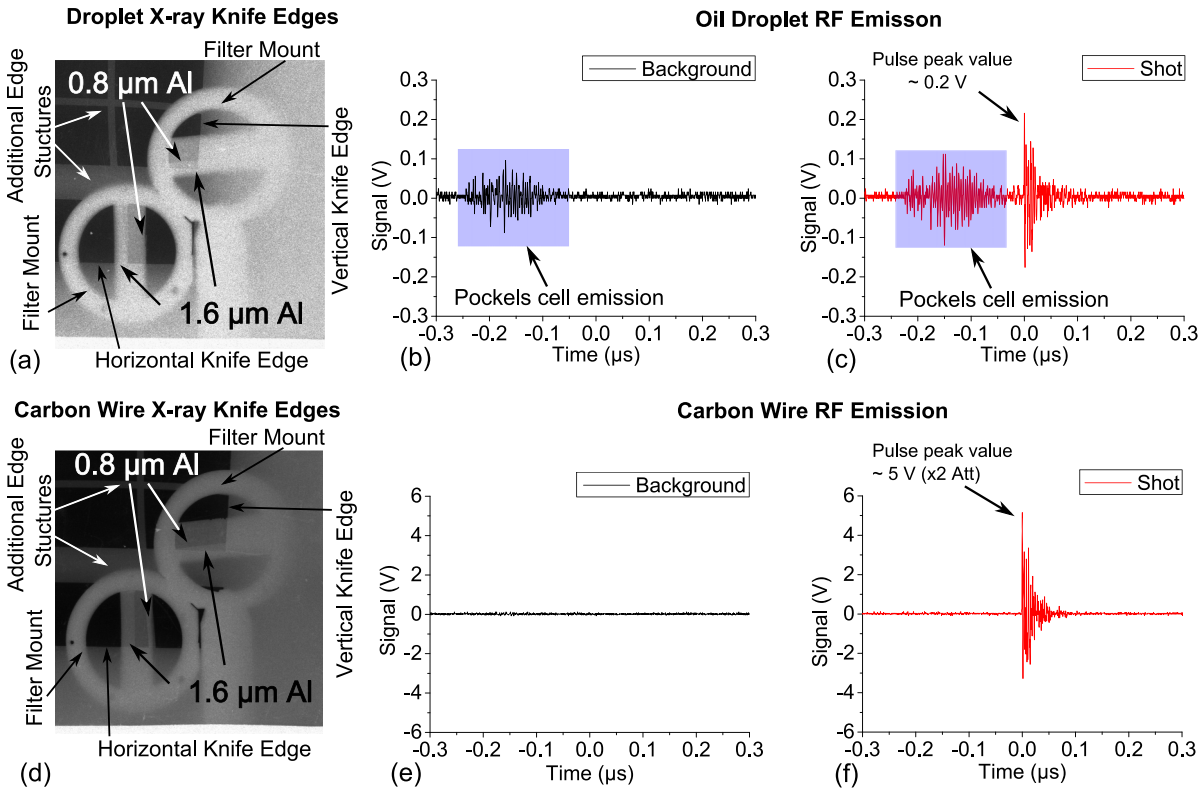

FIG. 6. (a) and (d) Filtered X-ray images from a levitated oil droplet and carbon wire target, showing horizontal and vertical knife-edge shadows, alignment fiducial wires, and the shadows of the circular filter supports. The transmission through the 0.8 μm (>300 eV) and 1.6 μm (>400 eV) Al foil gave some indication of the relative photon energies being emitted from each target type. The low level of transmission through the 1.6 μm foil, from the droplet shot, was such that no edge could be sufficiently resolved to give a source size measurement. This also indicated lower energy X-rays being emitted from the droplet than compared to the carbon wire. The course grid structures at the top left of each image were from fine wires used for additional source size measurements, not included in the analysis presented here. RF emission measurements from a high-intensity laser irradiated droplet ((b) and (c)) and carbon wire ((e) and (f)) interaction. The droplet background and shot measurements record a small early time noise signal from a switched Pockels cell firing with the main laser, followed by a RF pulse generated by the laser-target interaction. The peak pulse value from the carbon wire shot was approximately 25 times larger than the peak value from the droplet shot and the integrated pulse from the carbon wire approximately 9 times larger than from the droplet.

inferred from the time integrated measurement. A more detailed investigation of this process and a comparison to a range of other target geometries will be the subject of future experiments beyond the scope of the droplet source development presented here.

B. RF emission

Figures 6(b), 6(c), 6(e), and 6(f) show the RF response measurements for the droplet and carbon wire. The summed background signal was deducted from the summed shot signal, and this value was used as a measure of the magnitude of the RF emission pulse. The background signal was taken as the measured pick up when the laser was fired into the chamber with no target in place. The start of the pulse duration was defined as the point where the voltage exceeded twice the noise level and the end of the pulse by the point where the signal remained within one standard deviation (noise) value of the baseline signal. The shot and background data from the droplet interaction show low-level pickup from the laser system switched Pockels cells which provided a useful early time marker and also indicated the relatively low levels of emission from the droplet. The peak value of the pulse from the droplet was measured to be approximately 0.2 V, with the total pulse duration of ~0.1 μs. This gave an integrated signal of around 226 V. The RF pulse from the carbon wire shot gave a peak value of approximately 5 V (with 2× attenuation), with the same pulse duration as the droplet emission. The RF pulse gave an integrated signal of ~1980 V, roughly 9 times larger than the emission pulse from the droplet. As the droplet was of a comparable size and atomic composition to the carbon wire, the lower level of emission indicated that this was a

TABLE I. Filtered (0.8 μm Al) X-ray source size measurements for a ~10 μm levitated oil microdroplet and a 9 μm carbon wire highlighting an extension of X-ray emission along the length of the wire target from thermal transport.

Target	Horizontal source size (μm)	Vertical source size (μm)
Droplet	20 ± 2	19 ± 3
Carbon wire	28 ± 3	20 ± 3

result of the droplet's physical isolation in space and not its size or composition.

V. CONCLUSIONS

A large working distance, vacuum-compatible optical-levitation trap was designed and built, and its application in preliminary high-intensity laser matter interaction studies successfully demonstrated. The use of a long working distance singlet focusing optic offered a unique trapping geometry and very large "free" solid angle availability that facilitated the use of multiple X-ray, plasma, and optical imaging diagnostics. Silicon oil microdroplets, of 10 ± 4 μm diameter, were trapped under atmospheric and vacuum conditions ($\sim 1.6 \times 10^{-1}$ millibars) for several hours at a time and a high speed (10 kHz sensor) optical imaging, and data acquisition system was developed to monitor the droplets position in real time, with a resolution of ~ 5 μm in vacuum. The stability of the optically trapped oil droplets demonstrated that this type of target can be held within the focal spot size of an irradiating beam (~ 7 μm), long enough to be well aligned to the heating beam (~ 5 min). Measurements of X-ray source size, multi-keV photon energy spectrum, and RF emission of laser-heated levitated droplets were carried out, providing additional motivation for further investigation of this unique type of target in high-intensity laser interaction studies. In future experiments, detailed comparisons will be made between levitated droplet targets and a comprehensive set of alternative targets with a greater range of size and composition in order to better determine the extent to which the geometry and atomic mix of the target influences the X-ray source size and photon energy. To better characterise the RF emission, as described by Aspiotis *et al.*,[41] a more detailed investigation into the spectral composition, pulse duration, and radiated intensity over a large temporal and spectral range will be required.

ACKNOWLEDGMENTS

We are pleased to acknowledge the support of C. J. Price via an EPSRC studentship and for equipment loan and donations from AWE Aldermaston. S. Giltrap and N. Stuart were supported by AWE/EPSRC CASE studentships and S. Patankar by EPSRC KTS Fellowship No. RSRO P43480.

[1]L. Rymell and H. M. Hertz, Opt. Commun. **103**, 105 (1993).
[2]M. Anand, C. P. Safvan, and M. Krishnamurthy, Appl. Phys. B **81**, 469 (2005).
[3]M. Anand, S. Kahaly, G. Ravindra Kumar, M. Krishnamurthy, A. S. Sandhu, and P. Gibbon, Appl. Phys. Lett. **83**, 181111 (2006).
[4]J. Zheng, Z. Sheng, X. Peng, and J. Zhang, Phys. Plasmas **12**, 113105 (2005).
[5]T. D. Donnelly, M. Rust, I. Weiner, M. Allen, R. A. Smith, C. A. Steinke, S. Wilks, J. Zweiback, T. E. Cowan, and T. Ditmire, J. Phys. B: At., Mol. Opt. Phys. **34**, L313 (2001).
[6]D. R. Symes, A. J. Comley, and R. A. Smith, Phys. Rev. Lett. **93**, 145004 (2004).
[7]E. T. Gumbrell, A. J. Comley, M. H. R. Hutchinson, and R. A. Smith, Phys. Plasmas **8**, 1329 (2001).
[8]M. Schnurer, S. Ter-Avetisyan, S. Busch, E. Risse, M. P. Kalachnikov, W. Sander, and P. V. Nickles, Laser Part. Beams **23**, 337 (2004).
[9]J. Limpouch, J. Psikal, A. A. Andreev, K. YU. Plantonov, and S. Kawata, Laser Part. Beams **26**, 225 (2008).
[10]A. Henig, D. Kiefer, M. Geissler, S. G. Rykovanov, R. Ramis, R. Horlein, J. Osterhoff, Zs. Major, L. Veisz, S. Karsch, F. Krausz, D. Habs, and J. Schreiber, Phys. Rev. Lett. **102**, 095002 (2009).
[11]T. Sokollik, M. Schnurer, S. Steinke, P. V. Nickles, W. Sandner, M. Amin, T. Toncian, O. Willi, and A. A. Andreev, Phys. Rev. Lett. **103**, 135003 (2009).
[12]C. G. Brown, Jr., E. Bond, T. Clancy, S. Dangi, D. C. Dger, W. Ferguson, J. Kimbrough, and A. Throop, J. Phys.: Conf. Ser. **244**, 032001 (2010).
[13]C. G. Brown, Jr., T. Clancy, D. C. Eder, W. Ferguson, and A. Throop, EPJ Web Conf. **59**, 08012 (2013).
[14]L. C. Mountford, R. A. Smith, and M. H. R. Hutchinson, Rev. Sci. Instrum. **69**, 3780 (1998).
[15]D. P. DePonte, U. Weierstall, D. Starodub, K. Schmidt, J. C. H. Spence, and R. B. Doak, J. Phys. D: Appl. Phys. **41**, 195505 (2008).
[16]H. A. Sumeruk, S. Kneip, D. R. Symes, I. V. Churina, A. V. Belolipetski, T. D. Donnelly, and T. Ditmire, Phys. Rev. Lett. **98**, 045001 (2007).
[17]T. Sokollik, T. Paasch-Colberg, K. Gorling, U. Eichmann, M. Schurer, S. Steinke, P. V. Nickles, A. Andreev, and W. Sandner, New J. Phys. **12**, 113013 (2010).
[18]T. Paasch-Colberg, T. Sokollik, K. Gorling, U. Eichmann, S. Steinke, M. Schnurer, P. V. Nichles, A. Andreev, and W. Sandner, Nucl. Instrum. Methods Phys. Res., Sect. A **653**, 30 (2011).
[19]L. Rayleigh, Philos. Mag. Ser. 5 **14**, 184 (1882).
[20]E. F. Nichols and G. F. Hull, Phys. Rev. (Ser. I) **13**, 307 (1901).
[21]P. N. Lebedev, Ann. Phys. **311**, 433 (1901).
[22]A. Ashkin, Phys. Rev. Lett. **24**, 156 (1970).
[23]A. Ashkin and J. M. Dziedzic, Science **187**, 1073 (1975).
[24]A. Ashkin and J. M. Dziedzic, Appl. Phys. Lett. **24**, 586 (1974).
[25]A. Ashkin and J. M. Dziedzic, Appl. Phys. Lett. **28**, 333 (1976).
[26]Y. Arita, M. Mazilu, and K. Dholakia, Nat. Commun. **4**, 2374 (2013).
[27]H. Kapteyn and M. Murnane, Opt. Lett. **16**(7), 409 (1991).
[28]G. Doumy, F. Quere, O. Gobert, M. Perdrix, and Ph. Martin, Phys. Rev. E **69**, 026402 (2004).
[29]G. T. Tamura and A. G. Wilson, ASHRAE Trans. **73**, 170 (1967).
[30]M. Khoukhi and A. Al-Maqbali, Energy Procedia **6**, 422 (2011).
[31]J. Y. Kim and J. S. Kim, Open J. Fluid Dyn. **3**, 241 (2013).
[32]A. Ashkin and J. M. Dziedzic, Appl. Phys. Lett. **30**, 202 (1977).
[33]F. Ehrenhaft, Z. Phys. **18**, 352 (1917).
[34]A. Ashkin and J. M. Dziedzic, Appl. Phys. Lett. **19**, 283 (1971).
[35]D. Bigourd, S. Patankar, S. I. Olsson Robbie, H. W. Doyle, K. Mecseki, N. Stuart, K. Hadjicosti, N. Leblanc, G. H. C. New, and R. A. Smith, Appl. Phys. B **113**, 627 (2013).
[36]M. J. Mead, D. Neely, J. Gauoin, R. Heathcote, and P. Patel, Rev. Sci. Instrum. **75**, 4225 (2004).
[37]H. Hamster, A. Sullivan, S. Gordon, and R. W. Falcone, Phys. Rev. Lett. **71**, 2725 (1993).
[38]F. Beg, E. Clark, M. Wei, A. Dangor, R. Evans, A. Gopal, K. Lancaster, K. Ledingham, P. McKenna, P. Norreys, M. Tatarakis, M. Zepf, and K. Krushelnick, Phys. Rev. Lett. **92**, 095001 (2004).
[39]F. N. Beg, M. S. Wei, E. L. Clark, A. E. Dangor, R. G. Evans, P. Gibbon, A. Gopal, K. L. Lancaster, K. W. D. Ledingham, P. McKenna, P. A. Norreys, M. Tatarakis, M. Zepf, and K. Krushelnick, Phys. Plasmas **11**, 2806 (2004).
[40]K. Quinn, L. Romagnani, P. Wilson, B. Ramakrishna, M. Borghesi, M. M. Notley, L. Lancia, J. Fuchs, O. Will, and R. G. Evans, CLF Annual Report (2007–2008), p. 56.
[41]J. A. Aspiotis, N. Barbieri, R. Bernath, C. G. Brown, M. Richardson, and B. Y. Cooper, Proc. SPIE **6219**, 621908 (2006).